A low band gap iron sulfide hybrid semiconductor with unique 2D $[Fe_{16}S_{20}]^{8-}$ layer and reduced thermal conductivity†

Min Wu,[a] Jessica Rhee,[a] Thomas J. Emge,[a] Hongbin Yao,[a] Jen-Hau Cheng,[b] Suraj Thiagarajan,[b] Mark Croft,[c] Ronggui Yang[b] and Jing Li*[a]

Received (in Berkeley, CA, USA) 28th September 2009, Accepted 22nd January 2010
First published as an Advance Article on the web 6th February 2010
DOI: 10.1039/b920118a

A low band gap iron sulfide hybrid semiconductor with unique layered structure and unusual iron coordination exhibits significantly reduced thermal conductivity.

Iron sulfide compounds have been studied extensively because of their important properties and their uses in many different areas. For example, iron sulfur clusters as biological functional groups have been found in over 120 distinct types of enzymes and proteins.[1,2] Owing to their remarkable functional and structural diversities these systems have been the focus of investigation[3] for biological electron transportation,[4,5] redox potential modification,[6] and proton/election transfer coupling.[7,8] Since the first reports on spontaneous self assembly of iron sulfur based clusters,[9,10] many new members of this family (zero-dimension) have been discovered, for example, dimeric $[Fe_2S_2]^{2+}$,[11,12] trimeric $[Fe_3S_4]^{+}$,[13] tetrameric $[Fe_4S_4]^{+}$ and $[Fe_4S_4]^{2+}$[14,15] and hexameric $[Fe_6S_6]^{2+}$ and $[Fe_6S_6]^{3+}$.[16] Examples of one-dimensional (1D) chains of $[FeS_x]$ polyhedra have been reported in three-dimensional (3D) compounds of $Ce_2Fe_{1.82}S_5$,[17] $La_2Fe_2S_5$[18] and $Ce_2Fe_2S_5$.[19] Two-dimensional (2D) layered structures of iron sulfides are relatively unexplored. One such example is the $ACuFeS_2$ family (A = Li, Na, K, Rb, Cs), in which Cu and Fe occupy the same crystallographic sites.[20–24]

In searching for new functional materials, our main endeavours over the past decade have been focusing on the design, synthesis and modification of crystalline inorganic–organic hybrid semiconductors. The successful incorporation of two distinctly different components into a single crystal lattice has enabled us to develop a brand new family of semiconductor materials having significantly enhanced properties and unprecedented new phenomena.[25–30] Herein we report a new hybrid iron sulfide structure built on a unique 2D $[Fe_{16}S_{20}]^{4-}$ layer and unusual iron coordination. The optical bandgap of this compound is estimated to be ~0.6–0.8 eV. The incorporation of organic amines and complex cations between the inorganic layers gives rise to significantly reduced thermal conductivity.

Single crystals of $[Fe(en)_3]_2{\cdot}[Fe_{16}S_{20}]{\cdot}enH_2$ were grown by reactions of $FeCl_2$ (0.50 mmol, 99.5%, Alfa Aesar), dimethylsulfoxide (DMSO) (71 μl, 1.0 mmol, 99.9%, Acros Organics) and ethylenediamine (8.0 ml, 99%, Acros Organics) in a Teflon-lined stainless steel autoclave. The reagents were mixed and stirred for 10 min prior to heating and the vessel was then sealed and heated at 200 °C in furnace for 7 days. The autoclave was subsequently allowed to cool to room temperature. The product was filtered off, washed with 80% ethanol and distilled water several times. The black plate-like crystals were then collected (~60% yield). Pure polycrystalline samples were prepared under a similar procedure at a temperature range of 180–200 °C (~70–80% yield). The single crystal X-ray diffraction analysis‡ revealed that the title compound is composed of a unique $Fe_{16}S_{20}$ layer, as shown in Fig. 1 (left). There are sixteen crystallographically independent Fe atoms within the layer, all of which are seven-coordinated, with four to S and three to Fe atoms. The Fe–S distances range from 2.230 to 2.325 Å, similar to those found in a number of iron sulfide binary phases.[31–34] The Fe–Fe bond lengths vary from 2.708 to 2.843 Å, highly comparable with those found in other FeS compounds of hypervalent Fe coordination, for example, 2.759 Å,[33] and 2.743, 2.877 Å.[34] The sulfur atoms were either 3- or 4-coordinated. The organic amines and $[Fe(en)_3]^{3+}$ complex cations are located between the adjacent layers, as seen in Fig. 1 (right), forming a sandwich like structure. It is worth to mention the existance of both a +2 (within the layer) and +3 (in the $Fe(en)_3$ complex) oxidation state of iron in this compound.[35]

X-Ray absorption experiment (XAS) was performed to confirm the valances of iron. Fig. 2 (top) shows the transition

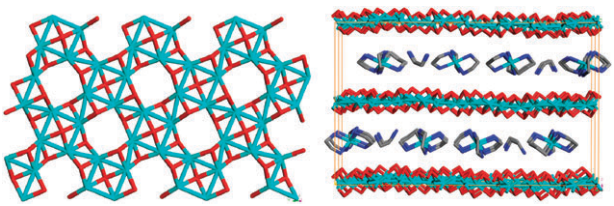

Fig. 1 View of a single layer of $[Fe_{16}S_{20}]^{4-}$ along the crystallographic *c* axis with *a* axis from left to right (left), and packing of $[Fe_{16}S_{20}]^{4-}$ layers along the crystallographic *a* axis with the *c* axis from left to right and with $[Fe(en)_3]^{2+}$ cations and ethylenediamine molecules residing between the layers (right). Color scheme: Fe and Fe associated bonds (light blue), S (red), N (blue), and C (grey).

[a] *Department of Chemistry and Chemical Biology Rutgers University, Piscataway, NJ 08854, USA. E-mail: jingli@rutgers.edu; Fax: (+01)732-445-5312*
[b] *Department of Mechanical Engineering University of Colorado at Boulder, Boulder, CO, USA*
[c] *Department of Physics and Astronomy Rutgers University, Piscataway, NJ 08854, USA*

† Electronic supplementary information (ESI) available: Details of the synthesis, experimental procedures, CIF, TGA, and thermal data. CCDC 750434 & 758084. For ESI and crystallographic data in CIF or other electronic format see DOI: 10.1039/b920118a

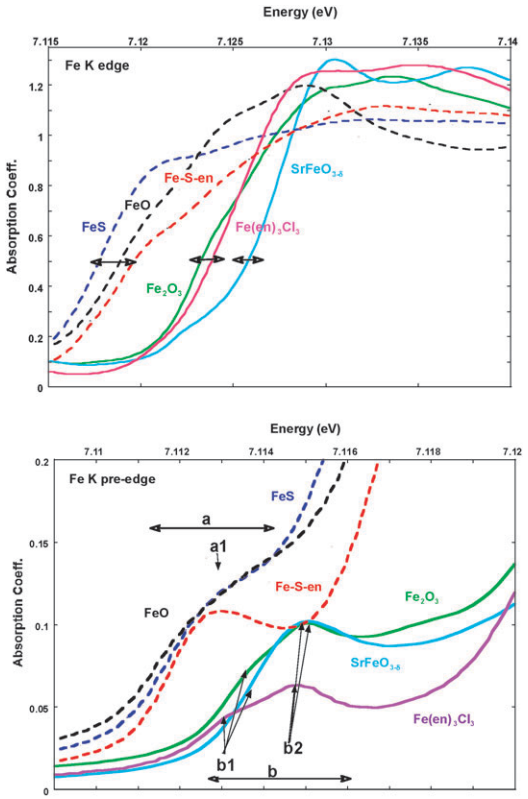

Fig. 2 Top: XAS spectra of Fe *K* edge for a series of Fe compounds with different Fe valances. Bottom: XAS spectra of Fe *K* Pre-edge. (Fe(II)S: dash blue, Fe(II)O: dash black, Fe–S–en (compound **3**): dash red, $Fe(III)_2O_3$: solid green, $Fe(III)(en)_3Cl_3$: solid purple, $SrFe(IV)O_{3-\delta}$: solid blue.

metal Fe *K*-edges. In general one expects a chemical shift to higher energy of an X-ray absorption edge with increasing formal chemical valence due to the loss of electronic screening with increasing valence. A number of factors, however, complicate this picture. The Fe *K* edge (see Fig. 2) marks the onset of dipole allowed transitions from the core-level 1s level to empty *p*-states. Both transitions to continuum states and atomic-like Fe-4p states dominate the Fe *K* near edge structure. In general there will be multiplicity of 4p states due to solid-state splittings of the 4p levels and by replication of 4p features associated with different 3d configurations which are covalently band mixed into the solid-state electronic structure. Thus the onset of the steeply rising portion of the edge will be influenced by 4p state splittings.

A good example of such splitting is provided by comparing the formally trivalent Fe_2O_3 and $Fe(en)_3Cl_3$. The $Fe(en)_3Cl_3$ has a smoothly rising edge whereas the Fe_2O_3 has a feature split down to lower energy and the peak features split to higher energy. The two spectra cross at an absorption coefficient of about 0.75 indicating their comparable chemical shift. The +4 compound $SrFeO_{3-\delta}$ can be seen to have a clearly higher chemical shift. The situation for the divalent compounds is somewhat more complicated. The divalent compounds FeO and FeS compounds clearly show edge shift to lower energy relative to the trivalent compounds, however, the difference in the near edge features of the two is rather widespread for the chemical shift in the divalent state. Moreover, the compound of interest here has a much lower symmetry than these standards precluding a direct simple comparison of their chemical shifts. Comparison of the inflection point of the initial rise in the title compound spectrum to the divalent standards can be said to support a "close to" divalent state for this compound.

In Fig. 2 (bottom), the Fe *K* pre-edge region is shown. Here the term pre-edge is used because these small features are shifted down in energy below the main edge. The features in this pre-edge region are due to quadrupole 1s to 3d transitions or dipole 1s to hybrid d/p states. The pre-edge features typically have semi-localized 3d final states which have an attractive Coulomb interaction with the 1s core hole created in the absorption process. This Coulomb energy accounts for the shifting of these features below the main edge. In general the Fe^{2+} spectra show pre-edge features in a lower energy range, labelled "a" in the inset, and the Fe^{3+}, Fe^{4+} pre-edge features occur in a somewhat higher "b" energy range. The Fe^{2+} pre-edge features are typically broader and unresolved. In contrast the Fe^{3+}/and Fe^{4+} pre-edge features typically show distinct b1–b2 sub features. The pre-edge feature of the title compound appears in structure and in energy consistent with a basically Fe^{2+} state. The quite high relative intensity of this compound pre-edge feature should be noted. The Fe in Fe–S–en sits in a non-centro-symmetric environment. This allows for d/p hybridization and the admixture of the stronger dipole 1s to p transitions into the pre-edge feature. Thus the high relative intensity of the Fe–S–en pre-edge feature is consistent with the low symmetry site.

Thermogravimetric (TG) experiments were carried out on powder samples of $[Fe(en)_3]_2{\cdot}[Fe_{16}S_{20}]{\cdot}enH_2$. Upon heating to 160 °C and holding this temperature for about an hour, the compound remained stable (Fig. S1–S2, ESI†). Continued heating gave a weight loss of ~19.9% up to 350 °C, which matches well with a calculated amount of ethylenediamine molecules (20.3%). Post TG structure analysis indicated Fe_9S_{10} as a major phase in the residue after being heated to 500 °C (Fig. S3†). The optical band gap of $[Fe(en)_3]_2{\cdot}[Fe_{16}S_{20}]{\cdot}enH_2$ was estimated from the room temperature diffuse reflectance spectrum. The values, ~0.6–0.8 eV, suggest that the compound is a low band gap semiconductor.

Thermal conductivity of $[Fe(en)_3]_2{\cdot}[Fe_{16}S_{20}]{\cdot}enH_2$ was measured on a pellet made by cold-pressing the powder under a pressure of 2500 atm. The thermal conductivity was determined by measuring the density, specific heat and thermal diffusivity separately (Fig. S4–S5, ESI†). The result of the thermal conductivity measurements is shown in Fig. 3. Compared to the thermal conductivity of FeS_2 (pyrite) and FeS (pyrrhotite), which are about 23 and 3.5 W/mK at 35 °C, respectively,[36] the title compound shows a considerably lower value of about 0.5–0.6 W/mK in the temperature range 25–100 °C.

In summary, a new type of iron sulfide hybrid material containing unique 2D $[Fe_{16}S_{20}]^{8-}$ layers has been successfully synthesized and characterized. The compound is a low band gap semiconductor with an estimated band gap of ~0.6–0.8 eV. The X-ray absorption study confirmed mixed valances of iron. In comparison with FeS binary phases, a significantly reduced thermal conductivity is achieved in

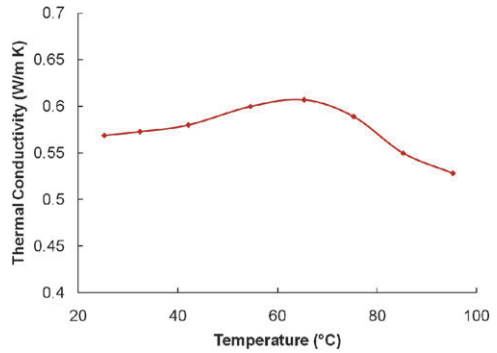

Fig. 3 Thermal conductivity of $[Fe(en)_3]_2{\cdot}[Fe_{16}S_{20}]{\cdot}enH_2$ as a function of temperature.

this compound, as a result of creating an organic–inorganic interface.

The authors are grateful to the National Science Foundation for the financial support through Grant No. DMR-0706069. We thank Dr Xiaoying Huang and Dr Ruibo Zhang for their contributions to this work.

Notes and references

‡ Crystal data of $[Fe(en)_3]_2{\cdot}[Fe_{16}S_{20}]{\cdot}enH_2$: C14 H58 Fe18 N14 S20, *fw* = 2069.24, Monoclinic, space group $P2_1/c$ (#14) with a = 8.3836(15), b = 33.209(6), c = 20.450(4) Å, β = 90.314(4)°, V = 5693.5(17) Å3, Z = 4, and ρcalc. = 2.414 gcm^{-3}. All measurements were made on a Bruker-AXS smart APEX CCD diffractometer at 100(2) K with graphite-monochromated Mo-Kα radiation. A total of 19 953 reflections were collected (7844 independent, R(int) = 0.0946) to a maximum θ of 23.34°). R_1 = 0.1089 ($I > 2\sigma(I)$), wR_2 = 0.1936 and GOF = 1.060. Largest diff. peak and hole 1.52 and −1.99 eÅ−3. CCDC 698828.

1 H. Beinert, *JBIC, J. Biol. Inorg. Chem.*, 2000, **5**, 2.
2 H. Beinert, R. H. Holm and E. Münck, *Science*, 1997, **277**, 653.
3 D. C. Johnson, D. R. Dean, A. D. Smith and M. K. Johnson, *Annu. Rev. Biochem.*, 2005, **74**, 247.
4 L. Noodleman and D. A. Case, *Adv. Inorg. Chem.*, 1992, **38**, 423.
5 T. Glaser, B. Hedman, K. O. Hodgson and E. I. Solomon, *Acc. Chem. Res.*, 2000, **33**, 859.
6 T. A. Link, *Adv. Inorg. Chem.*, 1999, **47**, 83.
7 W. N. Lanzilotta, J. Christiansen, D. R. Dean and L. C. Seefeldt, *Biochemistry*, 1998, **37**, 11376.
8 J. W. Peters, M. H. Stowell, S. M. Soltis, M. G. Finnegan, M. K. Johnson and D. C. Rees, *Biochemistry*, 1997, **36**, 1181.
9 B. A. Averill, T. Herskovitz, R. H. Holm and J. A. Ibers, *J. Am. Chem. Soc.*, 1973, **95**, 3523.
10 T. Herskovitz, B. A. Averill, R. H. Holm, J. A. Ibers, W. D. Phillips and J. F. Weiher, *Proc. Natl. Acad. Sci. U. S. A.*, 1972, **69**, 2437.
11 S. Han, R. S. Czernuszewicz and T. G. Spiro, *Inorg. Chem.*, 1986, **25**, 2276.
12 J. G. Reynolds and R. H. Holm, *Inorg. Chem.*, 1980, **19**, 3257.
13 K. S. Hagen, A. D. Watson and R. H. Holm, *J. Am. Chem. Soc.*, 1983, **105**, 3905.
14 S. Rutchik, S. Kim and M. A. Walters, *Inorg. Chem.*, 1988, **27**, 1515.
15 K. S. Hagen, A. D. Watson and R. H. Holm, *Inorg. Chem.*, 1984, **23**, 2984.
16 D. Coucouvanis, M. G. Kanatzidis, W. R. Dunham and W. R. Hagen, *J. Am. Chem. Soc.*, 1984, **106**, 7998.
17 W. Harms, A. M. Mills, T. Sohnel, C. Laubschat, F. E. Wagner, C. Geibel, Z. Hossain and M. Ruck, *Solid State Sci.*, 2005, **7**, 59.
18 F. Besrest and G. Collin, *J. Solid State Chem.*, 1977, **21**, 161.
19 M. Patrie, H. D. Nguyen and J. Flahaut, *C. R. Acad. Sci., Ser. C*, 1968, **266**, 1575.
20 J. Llanos, P. Valenzuela, C. Mujica, A. Buljan and R. Ramirez, *J. Solid State Chem.*, 1996, **122**, 31.
21 C. Mujica, J. Paez and J. Lianos, *Mater. Res. Bull.*, 1994, **29**, 263.
22 C. Mujica, J. Llanos, M. Guzman and C. Contreras-Ortega, *Nucleotecnica*, 1994, **14**, 23.
23 J. Llanos, C. Contreras-Ortega and C. Mujica, *Mater. Res. Bull.*, 1993, **28**, 39.
24 R. Fong, J. R. Dahn, R. J. Batchelor, F. W. B. Einstein and C. H. W. Jones, *Phys. Rev. B: Condens. Matter*, 1989, **39**, 4424.
25 X. Y. Huang, J. Li and H. Fu, *J. Am. Chem. Soc.*, 2000, **122**, 8789.
26 X. Y. Huang, H. R. Heulings IV, V. Le and J. Li, *Chem. Mater.*, 2001, **13**, 3754.
27 X. Y. Huang, J. Li, Y. Zhang and A. Mascarenhas, *J. Am. Chem. Soc.*, 2003, **125**, 7049.
28 X. Y. Huang and J. Li, *J. Am. Chem. Soc.*, 2007, **129**, 3157.
29 J. Li, W. H. Bi, W. Ki, X. Y. Huang and S. Reddy, *J. Am. Chem. Soc.*, 2007, **129**, 14140.
30 W. Ki and J. Li, *J. Am. Chem. Soc.*, 2008, **130**, 8114.
31 A. R. Lennie, S. A. T. Redfern, P. F. Schofield and D. J. Vaughan, *Mineral. Mag.*, 1995, **59**, 677.
32 R. J. Nelmes, M. I. McMahon, S. A. Belmonte and J. B. Parise, *Physical Review, B-Condensed Matter*, 1999, **59**, 9048.
33 J. Z. Jiang, R. K. Larsen, R. Lin, S. Morup, I. Chorkendorff, K. Nielsen, K. Hansen and K. West, *J. Solid State Chem.*, 1998, **138**, 114.
34 Y. Fei, C. T. Prewitt, D. J. Frost, J. B. Parise and K. Brister, *Rev. High Pressure Sci. Technol.*, 1998, **7**, 55.
35 J. Li, Z. Chen, R. J. Wang and D. M. Proserpio, *Coord. Chem. Rev.*, 1999, **190–192**, 707.
36 C. Clauner and E. Huenges, *Thermal Conductivity of Rocks and Minerals, Rock Physics and Phase Relations: A Handbook of Physical Constants*, ed. T. J. Ahrens, American Geophysical Union, Washington, D.C, 1995.